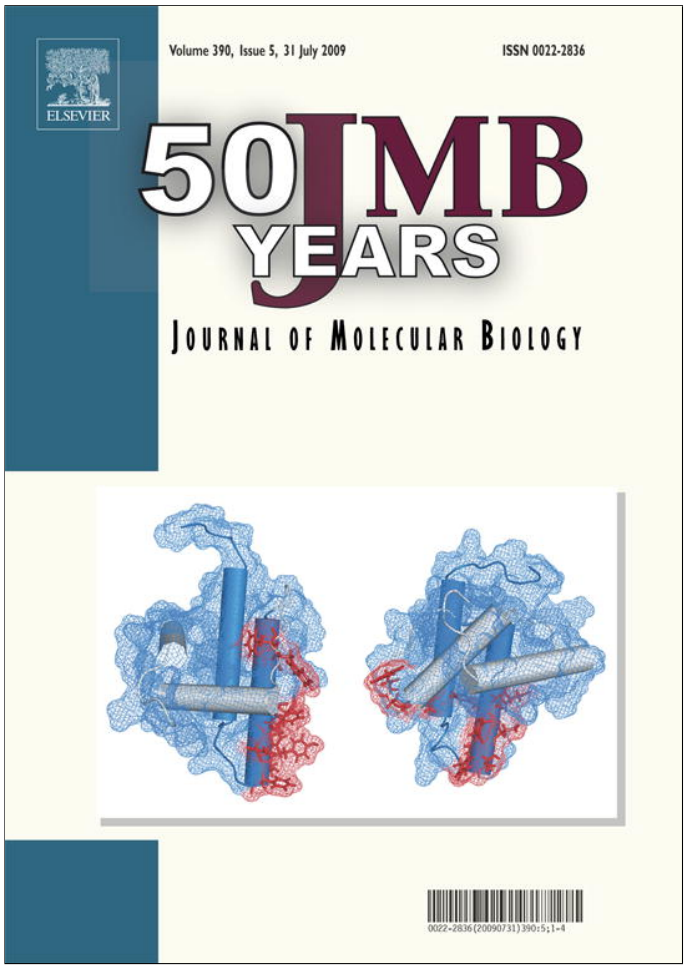

doi:10.1016/j.jmb.2009.06.002 J. Mol. Biol. (2009) 390, 1019–1029

JMB

Available online at www.sciencedirect.com

ScienceDirect

ELSEVIER

Mechanism for Attenuation of DNA Binding by MarR Family Transcriptional Regulators by Small Molecule Ligands

Inoka C. Perera, Yong-Hwan Lee, Steven P. Wilkinson and Anne Grove*

Department of Biological Sciences, Louisiana State University, Baton Rouge, LA 70803, USA

Received 23 April 2009; received in revised form 28 May 2009; accepted 1 June 2009
Available online 6 June 2009

Members of the multiple antibiotic resistance regulator (MarR) family control gene expression in a variety of metabolic processes in bacteria and archaea. Hypothetical uricase regulator (HucR), which belongs to the ligand-responsive branch of the MarR family, regulates uricase expression in *Deinococcus radiodurans* by binding a shared promoter region between *uricase* and *HucR* genes. We show here that HucR responds only to urate and, to a lesser extent, to xanthine by attenuated DNA binding, compared to other intermediates of purine degradation. Using molecular-dynamics-guided mutational analysis, we identified the ligand-binding site in HucR. Electrophoretic mobility shift assays and intrinsic Trp fluorescence have identified W20 from the N-terminal helix and R80 from helix 3, which serves as a scaffold for the DNA recognition helix, as being essential for ligand binding. Using structural data combined with *in silico* and *in vitro* analyses, we propose a mechanism for the attenuation of DNA binding in which a conformational change initiated by charge repulsion due to a bound ligand propagates to DNA recognition helices. This mechanism may apply generally to MarR homologs that bind anionic phenolic ligands.

Keywords: DNA binding; HucR; transcriptional regulator; tryptophan fluorescence; uric acid

Edited by M. Gottesman

Introduction

Ligand-responsive members of the multiple antibiotic resistance regulator (MarR) family of transcriptional regulators control a number of biological pathways in bacteria. They are involved in the regulation of the biosynthesis of virulence factors and the catabolism of environmental aromatic compounds, and many respond to antibiotics and oxidative stress.[1–3] The prototypical member of this family *Escherichia coli* MarR represses the expression of the *mar*RAB operon, which confers resistance to a variety of aromatic compounds, including antibiotics, organic solvents, and household disinfectants.[4–8]

Most MarR family repressors prevent gene expression by sterically hindering transcription. In ligand-responsive MarR family transcriptional regulators, derepression occurs when a conformational change in the protein, induced by association with a small-molecule ligand, lowers its affinity for cognate DNA, allowing transcription to proceed (for a review, see Wilkinson and Grove[3]).

Biochemical and biophysical studies designed to define the ligand specificity and conformational changes induced upon ligand binding to MarR homologs have yet to suggest a specific ligand-binding site or a mechanism by which a ligand would lower the affinity for cognate DNA.[9–12] Molecular structures of several MarR homologs, which assist in elucidating the mechanistic basis of DNA and ligand interaction, are available.[13–22] Although numerous studies have been carried out in order to identify the natural ligands of members of this vast family of transcriptional regulators, the mechanism of DNA binding antagonism upon ligand interaction remains elusive, as few structures have been solved both with and without a ligand bound. A recent structure of MTH313, a MarR-type

*Corresponding author. E-mail address: agrove@lsu.edu.
Present address: S. P. Wilkinson, Biomatrica, San Diego, CA 92121, USA.

Abbreviations used: MarR, multiple antibiotic resistance regulator; HucR, hypothetical uricase regulator; 5-HIU, 5-hydroxyisourate; PDB, Protein Data Bank; EMSA, electrophoretic mobility shift assay; WT, wild type; EDTA, ethylenediaminetetraacetic acid.

transcriptional regulator from *Methanobacterium thermoautotrophicum* solved both without ligand and with the ligand salicylate, provides evidence for displacement of the DNA-binding helix upon ligand binding,[22] while the originally suggested salicylate-binding site in *E. coli* MarR may have resulted from cocrystallization with high concentrations of the ligand.[13] Conformations incompatible with DNA binding have also been reported for *Pseudomonas aeruginosa* MexR in complex with its antirepressor ArmR and for oxidized *Xanthomonas campestris* OhrR.[23,24]

Hypothetical uricase regulator (HucR), a member of the MarR family of proteins encoded by *Deinococcus radiodurans*, participates in the purine degradation pathway by regulating urate oxidase expression.[25] HucR is a 39 kDa dimeric protein with the characteristic winged-helix domain for DNA binding. The two DNA-binding domains are spatially configured to interact readily with consecutive DNA major groves.[14] HucR binds with high affinity ($K_d \sim 0.3$ nM) to its operator sequence (*HucO*), which overlaps the promoter regions of the divergently oriented *HucR* and *urate oxidase* genes (Fig. 1a), repressing their expression. The natural ligand for HucR is urate; both *in vivo* and *in vitro* studies have shown that urate antagonizes HucR–*HucO* interaction, allowing the expression of *HucR* and *urate oxidase*.[25] Urate oxidase converts urate into the metastable 5-hydroxyisourate (5-HIU) by hydroxylation; 5-HIU is subsequently decarboxylated and oxidized spontaneously or enzymatically to form allantoin (Fig. 1b).[26–28] Notably, urate binds HucR with negative cooperativity, reflecting the presence of more than one ligand-binding site and suggesting a carefully controlled regulatory mechanism.[29] *D. radiodurans*, an extremely oxidative stress-resistant microorganism,[30] would benefit from retaining optimal levels of the antioxidant urate in its cytoplasm; tight regulation of uricase expression is therefore required, as excess urate would be deleterious due to its low solubility. Consistent with this interpretation, the genomic locus containing divergently oriented *HucR* and *urate oxidase* genes is unique to *D. radiodurans*.

There are only a few ligand-bound structures of MarR family proteins that are available in the Protein Data Bank (PDB); thus, a global regulatory mechanism by members of this family has yet to be delineated. Here we use site-directed mutagenesis guided by molecular modeling to define the urate-binding site in HucR. A functional model for DNA binding antagonism upon interaction with urate that likely applies to other MarR homologs binding small-molecule ligands is proposed.

Results

Only urate and xanthine antagonize HucR–*HucO* complex formation

To investigate the ligand specificity of HucR, we focused on compounds that are intermediates in the purine degradation pathway (Fig. 1c). Considering that HucR regulates the expression of uricase, which participates in the conversion of urate into allantoin, one expectation was for allantoin to be unable to attenuate DNA binding by HucR. DNA binding antagonism upon the addition of ligands was measured using electrophoretic mobility shift assays (EMSAs) (Fig. 2) in which HucR–*HucO* complex formation was challenged with increasing concentrations of selected ligands (urate, hypoxanthine, xanthine, allantoin, and adenine). Only urate and xanthine, the immediate precursor of urate in the purine degradation pathway, demonstrated a concentration-dependent antagonism towards HucR–*HucO* complex formation, having inhibition constants of 0.78±0.10 mM and 6.33±1.35 mM, respectively, indicating that urate disrupts HucR–*HucO* interaction at ~8-fold-lower concentrations compared to xanthine (Fig. 2a and b). None of the other ligands, including allantoin, demonstrates such an effect in this concentration range. Guanine could not be included in these assays due to

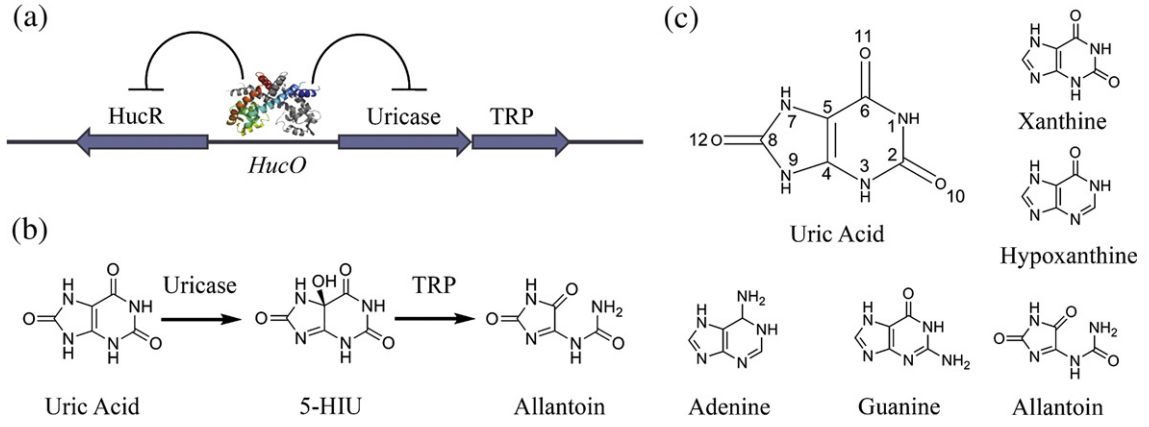

Fig. 1. (a) HucR binds to the operator sequence overlapping the promoters for divergently oriented genes encoding HucR and uricase, repressing their expression. (b) Uricase (urate oxidase) catalyzes the conversion of uric acid into 5-HIU, which either breaks down to allantoin spontaneously or catalyzed by transthyretin-related protein (TRP). (c) Ligands used in this study. Ligands represent intermediates in the purine degradation pathway.

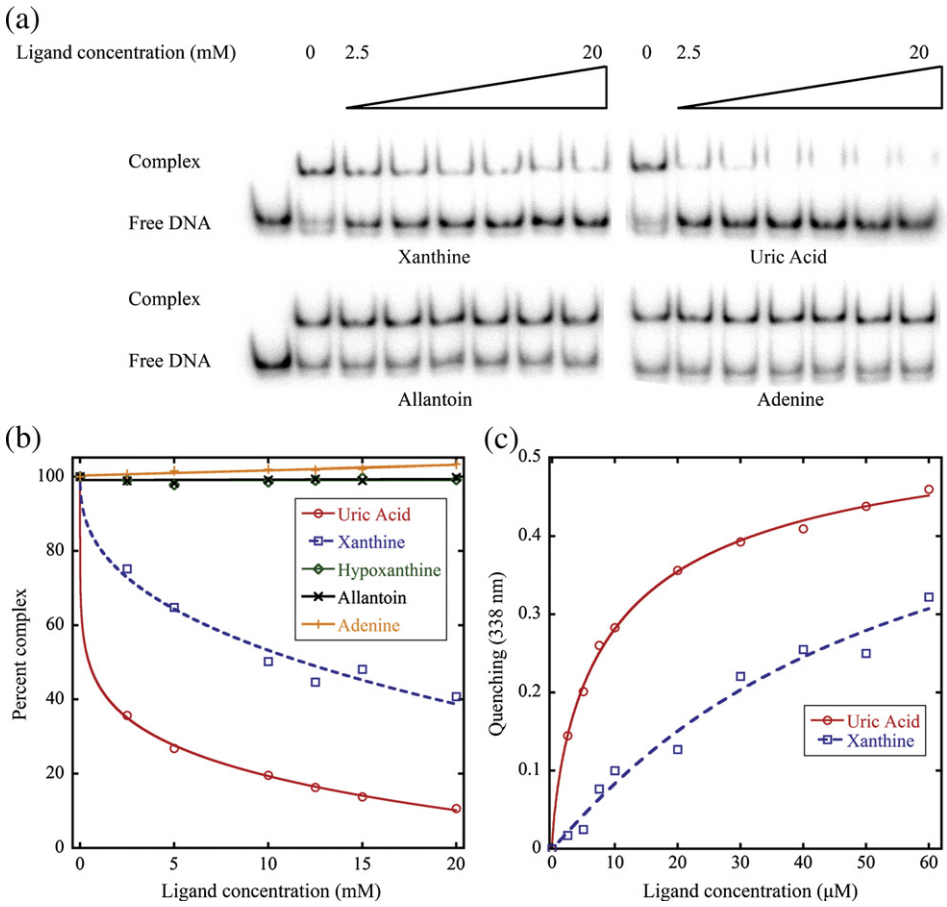

Fig. 2. Urate and xanthine attenuate HucR–*HucO* complex formation. (a) HucR–*HucO* complexes were challenged with 2.5–20 mM identified ligands to determine their effect on complex formation. (b) Densitometric data from (a) fitted to a two-component exponential decay, where urate (red open circle) shows an ~8-fold-higher capacity to disrupt the complex formation between HucR and *HucO* compared to xanthine (blue open square, broken line). (c) Quenching of HucR intrinsic fluorescence as a function of increasing concentrations of urate (red open circle) and xanthine (blue open square, broken line).

limitations in solubility under the current conditions. Furthermore, none of the pyrimidines (cytosine, uracil, or thymine) was able to reduce HucR–*HucO* binding (data not shown).

HucR contains two tryptophan residues per monomer and exhibits an intrinsic fluorescence that is quenched upon addition of urate.[29] As reported previously, fitting urate-mediated fluorescence quenching at the fluorescence emission maximum of 338 nm to the Hill equation revealed negative cooperativity, with $K = 10.58 \pm 2.01$ μM and $n_H = 0.75 \pm 0.07$. Notably, the only other ligand that is capable of eliciting fluorescence quenching is xanthine, which has a lower affinity and shows no cooperativity in binding ($K = 47.65 \pm 10.72$ μM and $n_H = 1.08 \pm 0.15$) (Fig. 2c). Taken together, these data indicate that only urate and xanthine can associate with HucR to attenuate DNA binding.

Blind docking predicts two ligand-binding sites per monomer

That uric acid binds to HucR with negative cooperativity predicts that there is more than one binding site per HucR dimer. The significant Trp fluorescence quenching in response to the addition of urate reflects an altered environment of one or both tryptophans; W20 is located in the N-terminal helix, which has no counterpart in the structures of reported MarR homologs, and W72 is in helix 3, which appears to form a scaffold for helices 4 and 5 that constitute the helix–turn–helix motif. An altered environment of W72 on urate binding might therefore seem intuitively logical, as helix 3 contacts the helix–turn–helix motif. However, W72 stacks on Y62, predicting instead that the primary source of HucR intrinsic fluorescence is W20.

To predict the sites of urate binding to HucR, we used the program suite AutoDock,[31] which is commonly used to predict how small-molecule ligands interact with their receptors. Ligand-bound structures of *E. coli* MarR[13] and *M. thermoautotrophicum* MTH313[22] were used as controls; while docking of *E. coli* MarR with salicylate did not return the binding pocket suggested by the crystal structure, MTH313 probed with salicylate predicted binding sites that overlay the actual ligand-bound structure with significant accuracy (data not shown). The primary site, the occupancy of which results in displacement of the DNA recognition helix, is

predicted as a high-affinity site, while the other site is one of several sites predicted by AutoDock to be a low-affinity site.

The surface of HucR was probed with its natural ligand uric acid, and two binding sites predicted per monomer were further examined to determine which residues may be involved in binding urate at the particular site (Fig. 3). In the inner binding site, W20 is at hydrogen-bonding distance to O11, while a salt bridge is predicted between R80 and the delocalized negative charge on O10, resulting from deprotonation of the N3 of uric acid (Fig. 3b). The negatively charged D73 would be repelled by the deprotonated N3 of urate. This association of urate would be consistent with the observed Trp fluorescence quenching on ligand binding. Upon further examination of the structure obtained in the absence of ligand, it is evident that R106 from the recognition helix and D73 contact each other. The delocalized opposite charges result in a salt bridge interaction (a 2.8 Å distance between D73 and R106) that would likely be affected upon binding of urate. As discussed below, binding of urate may alter the electrostatic environment in the binding pocket to promote an interaction between D73 and R106 that alters the disposition of the DNA recognition helix.

Closer examination of the outer binding site reveals R137 to be at a hydrogen-bonding distance to urate (Fig. 3c). The outer binding site is in close proximity to the inner binding site in space and is expected to be affected by the occupancy of the inner binding site, perhaps contributing to the observed negative cooperativity of urate binding.

Only the inner ligand-binding site is biologically relevant

To determine whether residues in the inner and outer binding sites predicted to contact urate indeed serve this function, we mutated each of these residues to the respective amino acids as follows: W20 to F, R80 to S, R137 to S, and D73 to S. Arginine 106, which makes a salt bridge contact with D73, was mutated to asparagine, hypothesizing that it would prevent the propagation of the ligand-binding signal to the recognition helix. All protein variants were purified to apparent homogeneity (Fig. 4a). Except for R106N, the single amino acid substitutions changed the DNA binding affinity by less than a factor of 3 compared to wild-type (WT) HucR (Table 1), and the specificity of binding was

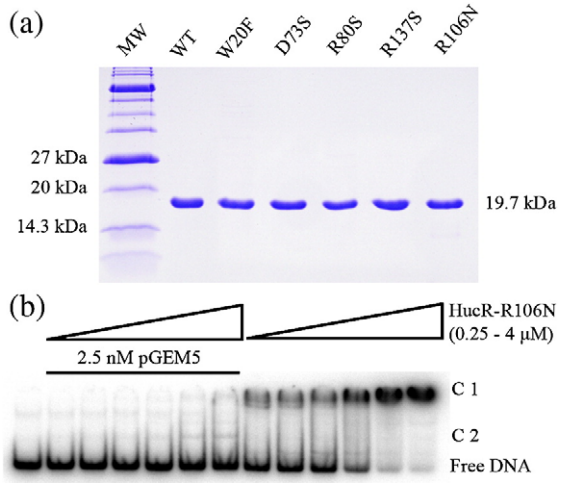

Fig. 4. (a) WT HucR and single-residue mutants were purified to >95% homogeneity. Molecular weight (MW) markers are indicated on the left. (b) *HucO* (0.1 nM) binding to HucR-R106N at concentrations of up to 4 μM. Complexes were challenged with a 25-times-higher concentration of the nonspecific competitor pGEM5 (left), revealing an unstable specific complex (C2) and a nonspecific complex (C1).

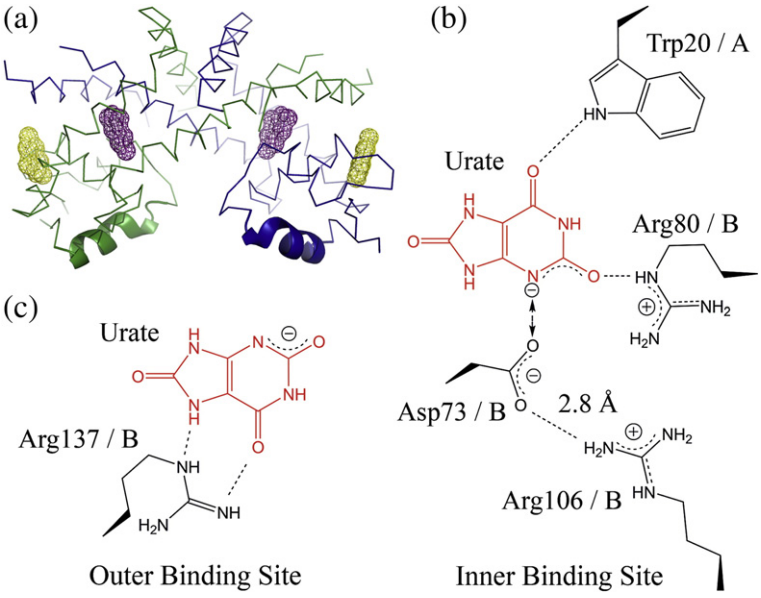

Fig. 3. Results of the blind docking of HucR using its natural ligand, uric acid. (a) The most probable binding sites on HucR were predicted using uric acid as ligand. The two binding sites with the lowest free energy were named inner binding site (purple) and outer binding site (yellow). DNA recognition helices are indicated in cartoon representation. (b) When urate is docked, W20 is at hydrogen-bonding distance to O11 of urate, R80 is predicted to form a salt bridge to O10, while deprotonated N3 repels D73 in the inner binding site. A salt bridge between D73 and R106 of the recognition helix is seen in the crystal structure. (c) In the outer binding site, R137 may hydrogen bond to urate through the hydrogen on N7 and O11. (b) and (c) show only predicted side-chain contacts of residues in the inner and outer binding sites; contacts with the peptide backbone are omitted for clarity.

Table 1. Dissociation constants of HucR variants

HucR variant	K_d (nM)
WT HucR	0.60±0.17
HucR-W20F	1.65±0.27
HucR-R80S	0.41±0.02
HucR-D73S	0.29±0.04
HucR-R137S	0.75±0.15

The observed dissociation constants (K_d) of HucR variants binding to *HucO* were determined by an analysis of densitometric data obtained from EMSAs.

unaltered (data not shown). For WT HucR, stoichiometric titrations indicating that the protein is essentially fully active were performed in the past.[25] The current determination of K_d agrees with previously measured values indicating full activity of the protein preparations used here. However, mutation of R106 to asparagine significantly compromised both DNA binding affinity and specificity of HucR (Fig. 4b). While the affinity of WT HucR for its cognate site is 0.3 nM (at the lower salt concentration used for HucR-R106N), complex formation with HucR-R106N is seen only at micromolar concentrations and low salt concentrations. Furthermore, addition of pGEM5 as a nonspecific competitor leads to disruption of complexes, indicating that specificity is lost by the R106-to-N substitution (Fig. 4b). In contrast, pGEM5 does not disrupt complex formation with WT HucR.[25] Evidently, R106 is essential for proper disposition of DNA recognition helices.

The ability of urate to antagonize complex formation by WT and mutant HucR variants was determined by EMSA (Fig. 5a). While the outer binding site mutant HucR-R137S responds to increasing concentrations of urate by a gradual decrease in residual complex, all of the inner binding site mutants formed DNA complexes that could not be disrupted by addition of urate. These data argue against the outer binding site as a physiologically relevant ligand-binding site and suggest that the presence of all residues in the predicted inner binding site is vital to the antagonistic effect of urate (Fig. 5a and b), thus validating the site predicted by AutoDock.

Fluorescence profiles of mutant proteins show variable patterns within the scanned region from 320 nm to 360 nm (Fig. 5c). For the W20F mutant, residual fluorescence is almost negligible, suggesting that W20 is indeed the primary source of fluorescence in WT HucR and that W72 fluorescence is quenched by the neighboring tyrosine (Y62). Mutation of R137 and D73 results in overlapping fluorescence profiles yet comparatively lower fluorescence intensities at 338 nm, suggesting a change in the immediate environment of W20. For R80, which is adjacent to W20 in space, its substitution to serine would alter the charge density within the microenvironment of the tryptophan residue, evidently reducing its maximum fluorescence.

Titration of increasing concentrations of urate against HucR-R137S shows concentration-dependent fluorescence quenching at 338 nm and retention of negative cooperativity (Fig. 5d), suggesting that mutation of this residue does not eliminate urate interaction with the protein and consistent with the ability of urate to attenuate DNA complex formation (Fig. 5a). The intrinsic fluorescence of HucR-R80S is increased upon addition of urate, suggesting that substitution of R80 instead results in an altered interaction with the ligand, as reflected in the increased Trp fluorescence. The failure of HucR-R80S to respond to urate binding by a decrease in DNA binding affinity further argues for an altered association with the ligand compared to WT HucR. In contrast, mutation of D73 to S abolishes fluorescence quenching, suggesting that the charge repulsion between N3 deprotonated urate and aspartate is important for ligand binding to HucR. Titration of HucR-R106N with urate shows a concentration-dependent quenching of Trp fluorescence, indicating urate binding (data not shown). Considering the low-affinity DNA binding by HucR-R106N, it is possible that its conformation is more akin to that of urate-bound HucR. Taken together, our data indicate that the inner binding site predicted by AutoDock indeed represents the ligand-binding site in HucR.

Discussion

A number of proteins within the MarR family bind phenolic compounds to regulate either their metabolism or their export from the cell via efflux pumps. Even for the well-studied *E. coli* MarR, the mechanism by which ligands attenuate DNA binding is not known. Elucidation of this mechanism has been hampered not only by the fact that many homologs bind multiple ligands or that the preferred ligand is not known but also by complications associated with obtaining cocrystal structures of ligand-bound protein. For *E. coli* MarR, the high concentration of salicylate used for obtaining crystals is widely thought to have resulted in a nonspecific association with solvent-exposed sites and concomitant stabilization of the crystal lattice. Consistent with this interpretation, application of AutoDock to the prediction of salicylate-binding sites within *E. coli* MarR did not identify the published solvent-exposed sites. Furthermore, it was shown that mutation of HucR residues, which are seen to coordinate salicylate in MarR, does not significantly affect DNA binding or response to urate.[29] However, the MTH313 crystal structure with bound ligand closely overlaps with the results from blind docking with salicylate, indicating that this program suite can be utilized to probe for ligand-binding sites in MarR homologs. Encouraged by the ability of AutoDock to predict the crystallographically identified salicylate-binding site in MTH313, we therefore probed the surface of HucR with uric acid to predict its cognate site.

Molecular docking suggests two possible ligand-binding sites per HucR monomer (Fig. 3). In the inner binding site, residues W20 and R80 contact O10 and O11 of urate through hydrogen-bonding or

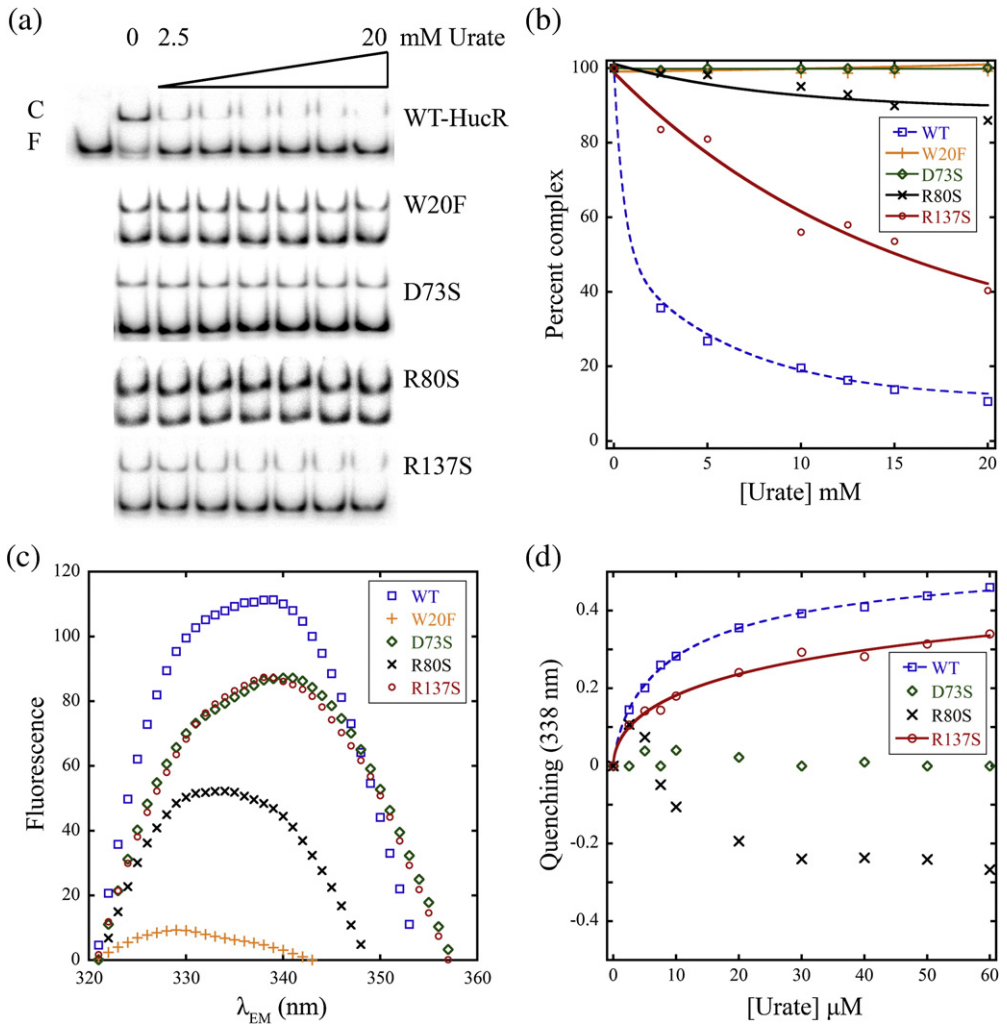

Fig. 5. (a) HucR–*HucO* complexes with WT and the HucR variants D73S, W20F, R80S, and R137S were challenged with 2.5–20 mM urate. (b) Densitometric data from EMSA were fitted to a two-component exponential decay. WT HucR (blue open squares, blue broken line) and HucR-R137S (red open circle, red line) complexes with *HucO* can be disrupted with urate. (c) Fluorescence profiles of HucR mutants. Mutation of W20 to F (orange plus signs) causes a significant loss in the intrinsic fluorescence of HucR. Compared to WT HucR, HucR-R80S (black crosses), HucR-D73S (green diamonds), and HucR-R137S (red open circles) show low fluorescence maxima at 338 nm. (d) Fluorescence quenching upon ligand interaction with HucR mutants. Similar to HucR WT (blue open squares, blue broken line), the outer binding site mutant HucR-R137S (red open circles, red line) shows concentration-dependent fluorescence quenching upon addition of urate. Mutation of D73 to S (green diamonds) abolishes responsiveness to urate, while the response is altered in the mutant HucR-R80S (black crosses).

electrostatic interactions, respectively. Under physiological conditions, N3 of uric acid would be deprotonated ($pK_a = 5.8$),[32] causing delocalization of the resulting negative charge. We speculate that interaction with the abovementioned side chains, along with contacts with the peptide backbone of T77, M41, and L44, allows the ligand to anchor in the inner ligand-binding site. In the crystal structure, D73 and R106 of the recognition helix are separated by 2.8 Å, allowing a salt bridge interaction.[14] Upon binding of urate, the spatial disposition of D73 ($pK_a = 3.9$) may change due to charge repulsion—a conformational change that would propagate due to the salt bridge interaction between D73 and R106 (Fig. 6). This interaction may change the orientation of the recognition helix, resulting in attenuated binding to *HucO*. Consistent with this interpretation, mutation of R106 in the recognition helix to N severely compromised the DNA binding affinity of HucR, demonstrating that it is an important residue required to anchor the DNA-binding helix in position. Thus, even a slight alteration of its position through propagation of ligand-induced conformational changes would compromise the interaction of the recognition helix with the cognate DNA.

Our proposed model posits that the salt bridge between D73 and R106 serves to orient the DNA recognition helix properly. While substitution of R106 to N severely compromises both DNA binding affinity and specificity, consistent with this interpretation, substitution of D73 to N has little to no effect on DNA binding. Examination of the HucR structure reveals multiple contacts of the guanidino groups of arginine.[14] One guanidino nitrogen is

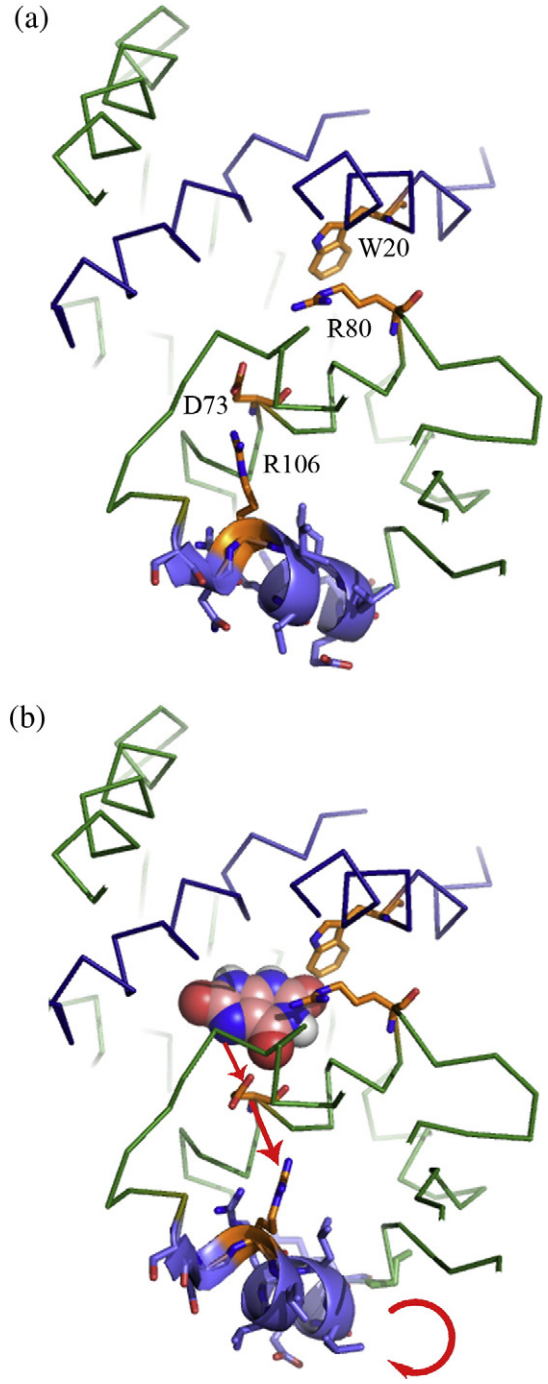

Fig. 6. (a) Proposed model for the antagonistic effect of urate on HucR–DNA interaction. In the illustrated single ligand-binding site of HucR, blue and green ribbons represent the contribution of either monomer to the formation of the binding site. The recognition helix (blue) is in cartoon representation, while the residues discussed in this work are in stick form, with carbon atoms shown in orange. (b) Upon binding of urate (spheres), repulsion of D73 may displace R106 of the recognition helix, causing a conformational change in the recognition helix that alters the face presented to the DNA major groove.

3.1 Å away from the backbone carbonyl of A70, while the other is 3.5 Å away from the side chain of T103. Thus, R106 is anchored by multiple contacts and, as a result, substitution of D73 does not compromise its disposition.

The proposed mechanism is consistent with the ligand specificity of HucR. Both the delocalized negative charge and the hydrogen-bond donor and acceptor atoms characteristic of urate may be important for the ligand to bind and induce the conformational change required to produce a protein conformation incompatible with DNA binding. Although xanthine hosts hydrogen-bond donor and acceptor atoms similar to those of uric acid, it is less efficient at antagonizing DNA binding. This may be due to the absence of polar O12, which would prevent xanthine from contacting the backbone of L44, as seen with docked uric acid, decreasing its affinity for the binding site. Furthermore, xanthine would be expected to be only partially deprotonated under these reaction conditions ($pK_a = 7.44$).[33] As a negative charge on N3 would be required for the proposed unfavorable interaction with D73, the only partial deprotonation of xanthine would be consistent with its reduced efficiency in attenuating HucR–DNA complex formation. Consistent with this interpretation, hypoxanthine ($pK_a = 8.94$),[33] which has no charge on N3, fails to bind HucR and does not affect complex formation. This is also consistent with the nonresponsiveness of HucR–*HucO* complex formation to thymine and uracil ($pK_a = 9.9$ and $pK_a = 9.5$, respectively),[33] which feature carbonyl groups in positions similar to those in xanthine but lack charge.

While complex formation by HucR-R80S is unaffected by bound ligand, Trp fluorescence data suggest that urate still binds to HucR-R80S. It is conceivable that urate reverses orientation by a 180° rotation about its long axis to prevent repulsion between N3 of urate and D73; such an orientation of the ligand would be precluded in WT HucR due to the interaction between the ligand and R80. In contrast, mutation of D73 to S abolishes fluorescence quenching, suggesting that the ligand no longer interacts with this mutant, consistent with the lack of complex perturbation upon ligand addition. The D73S variant also exhibits an intrinsic fluorescence lower than that of WT HucR, indicating an altered environment of W20. We therefore surmise that removal of the negative charge results in a restructuring of the ligand-binding pocket that is sufficient to prevent urate binding. Although a second Trp is present (W72) in the W20F mutant, the protein shows an extremely low emission at 338 nm. This may be due to W72 fluorescence quenching by neighboring Y62 and H147 that flank W72 at a distance of 4.2 Å and 3.7 Å, respectively. Mutation at the suggested outer binding site results in neither a change in the dissociation of complex upon ligand binding nor a change in binding, as suggested by fluorescence quenching within the range of concentrations tested. This likely reflects that this site is not physiologically relevant.

Urate docked in the inner binding site contacts the carbonyl oxygens of L44 and M41 of the long dimerization helices α2 or α2′ from either monomer of

HucR. Repulsion between the polar O12 of urate and the carbonyl oxygen of L44, which makes a hydrophobic interaction with L54′ (of the other dimerization helix), along with hydrogen bonding between the carbonyl oxygen of M41 and N7-H of urate, may cause a conformational alteration that has the potential to propagate to the mirror-binding site in the other monomer. Such induced conformational changes could lower the binding affinity of the second binding site, causing the observed negative cooperativity. This is consistent with our previous inference that negative cooperativity is observed between high-affinity ligand sites.[29] That xanthine is missing O12 would be consistent with the inability of this ligand to elicit negative cooperativity.

The recently published structure of MTH313,[22] a MarR-like protein from *M. thermoautotrophicum* with unknown physiological function, offered the first opportunity to compare the structures of an unbound MarR homolog with that of the protein in complex with a small-molecule ligand. The MTH313 crystal structure shows asymmetry in ligand-binding sites, where the first binding site is located at the DNA-binding and dimerization domains and where the binding site within the other monomer is at a distant site that is more solvent exposed.[22] It was speculated that such a configuration of ligand-binding sites might function to accommodate diverse ligands. Structural alignment of salicylate-bound MTH313 and urate-docked HucR (RMSD = 3.14 Å for 263 common C^{α} residues) reveals that the inner binding site of HucR superimposes well with the first binding site of MTH313, which was suggested to be biologically relevant because it imposes the greatest structural alteration upon ligand binding (Fig. 7). This is particularly noteworthy as HucR uses W20 from its N-terminal helix to coordinate the ligand; this structural element is absent from MTH313. Furthermore, the salicylate-bound structure of SlyA from *Salmonella typhimurium* (PDB 3DEU; P. S. Brzovic, *et al.*, unpublished data) also shares this binding pocket predicted for HucR, showing that this may be a structurally analogous binding site shared by members of the MarR family of transcriptional regulators.

The natural ligand for many MarR family transcriptional regulators is elusive due to low affinity or a wide range of ligands that are able to cause derepression. For HucR, the selective binding of one principal ligand was anticipated based on its physiological role in regulating uricase expression. Consistent with this expectation, we find that HucR only responds to urate and, to a lesser extent, to xanthine, the immediate precursor to urate in the purine degradation pathway. HucR therefore serves as a model to analyze MarR family transcriptional regulators and their interactions with ligands, particularly the mechanism by which ligand mediates derepression. The model for the ligand-induced DNA binding antagonism proposed here likely extends to other MarR homologs, many of which bind anionic phenolic ligands.[3]

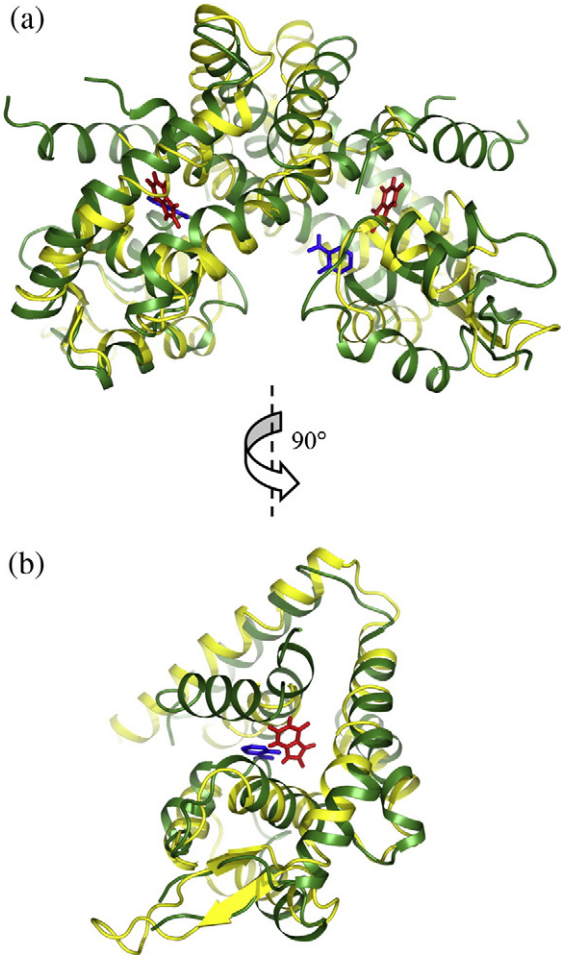

Fig. 7. (a) Overlap of salicylate-bound MTH313 (yellow) and urate-docked HucR (green). Ligands in the binding sites (urate and salicylate) are shown in red and blue, respectively. Salicylate-binding sites on MTH313 are asymmetric in the crystal structure, while predicted inner binding sites on HucR are symmetric. (b) A view of the structural alignment rotated 90° counterclockwise about the middle vertical axis shows the conserved binding pocket for urate and salicylate.

Materials and Methods

Construction and purification of mutant proteins

Residues predicted by *in silico* docking were mutated by whole plasmid PCR amplification using template pSW1,[25] in which the gene encoding HucR was cloned between EcoRI and NdeI sites in the vector pET5a. W20 was replaced by phenylalanine using the mutagenic forward and reverse primers 5′-G AGC GGA **TTC** GGA GCG ACT TCG C/5′-CA GAA GGG CTG CCG TGT CGT TGT C; D73 was replaced by serine using 5′-CG GGC TGG **AGC** CTG CTG CTC A/5′-C CGC GTT CAG CCC CGA AGC; R80 was replaced by serine with 5′-CG CTT TAC **AGC** TCG GCG CCG/T GAG CAG CAG GTC CCA GCC CG;

R137 was replaced by serine with 5′-G CAG GGC **AGC** GCC CTG GT/5′-GG CGT CAG GCG AAT ACT CGC CGA; and R106 was replaced by asparagine with 5′-ACG AGC AAC **AAT** ATC GTG CGG C/5′-CGA AGG CCC GGA AAT GGC (mutated codons in boldface). Resultant PCR products were transformed into *E. coli* NovaBlue (Novagen) electrocompetent cells, and the integrity of the constructs was confirmed by sequencing. Extracted plasmids were then transformed into *E. coli* BL21(DE3) pLysS for overexpression of proteins.

All proteins were purified to >95% purity with modifications to the procedure published for the purification of WT HucR.[25] Cells were grown in Luria–Bertani media supplemented with 100 μg/ml ampicillin and 50 μg/ml chloramphenicol. Protein was overexpressed for 1 h with 0.5 mM isopropyl β-D-1-thiogalactopyranoside when the cultures had reached an optical density of 0.5 at 600 nm. Culture flasks were kept on ice for 20 min before harvest of the cells by centrifugation. All subsequent steps were carried out at 4 °C. Cells were resuspended in lysis buffer [50 mM Tris–HCl (pH 8.0), 25 mM KCl, 5% glycerol (vol/vol), 5 mM Na_2 ethylenediaminetetraacetic acid (EDTA), 0.15 mM phenylmethylsulfonyl fluoride (PMSF), and 10 mM 2-mercaptoethanol] and lysed by treatment with 200 μg/ml lysozyme for 1 h. Lysis was completed with 0.05% Triton X-100 and immediate addition of 500 mM NaCl. DNA was precipitated by slow addition of 13% Polymin P to a final concentration of 0.5%, with constant stirring. After removal of precipitates by centrifugation, the protein in the supernatant was concentrated with 55% wt/vol $(NH_4)_2SO_4$. After centrifugation at 10,000*g* for 30 min, the pellet was resuspended in 10 ml of HAP-A buffer (pH 8.7) [50 mM Tris–HCl (pH 8.7), 25 mM KCl, 5% glycerol (vol/vol), 5 mM Na_2EDTA, 0.15 mM PMSF, and 10 mM 2-mercaptoethanol] and dialyzed overnight against 200 vol of HAP-A buffer. After centrifugation of the suspension, the supernatant was passed through tandem DEAE and CM Sepharose columns equilibrated in HAP-A buffer. Protein in the flow-through was then dialyzed against 200 vol of HEP-A buffer (pH 7.0) [20 mM potassium phosphate (pH 7.0), 25 mM KCl, 5% glycerol (vol/vol), 5 mM Na_2EDTA, 0.15 mM PMSF, and 10 mM 2-mercaptoethanol] for 4 h before passing through a hydroxylapatite column. The flow-through was then passed through a heparin column equilibrated with HEP-A buffer (pH 7.0). The proteins HucR-D73S, HucR-R106N, and HucR-R137S bound to this column and were eluted with a linear gradient of KCl from 50 mM to 1 M. The peak fractions were pooled and concentrated 10 times with a Centriprep centrifugal concentrating device (Millipore Corp.), and glycerol content was raised to 20% before storage of the proteins at −80 °C. Since HucR-W20F and HucR-R80S did not bind to the heparin column, the flow-through was collected, dialyzed against 200 vol of buffer (pH 6.0) [20 mM potassium phosphate (pH 6.0), 25 mM KCl, 5% glycerol (vol/vol), 5 mM Na_2EDTA, 0.15 mM PMSF, and 10 mM 2-mercaptoethanol], and run through a CM Sepharose column equilibrated with the same buffer. The pure desired protein was collected in the flow-through. Proteins were then concentrated as mentioned above, buffer exchanged with HAP-A buffer (pH 7.0), and stored as mentioned above. The concentration of purified proteins was determined using Micro BCA Protein Assay Kit (Pierce).

Prediction of ligand-binding sites

To assess the feasibility of using blind docking to predict the urate-binding site for HucR *in silico*, we utilized two MarR family proteins for which crystal structures are available in their ligand-bound form: *E. coli* MarR (PDB 1JGS)[13] and MarR-like protein MTH313 from *M. thermoautotrophicum*, for which both apo- and salicylate-bound structures (PDB 3BPV and 3BPX)[22] were utilized. Ligands and macromolecules were processed for docking using MGLTools 1.5.2,[31,34] while AutoDock 4† and AutoDock Vina 1.0 beta 03‡ were used to dock the ligands to selected proteins. Initial blind docking was carried out with large grid boxes enclosing the entire dimeric protein and, on subsequent rounds, enclosing more thermodynamically preferred sites.

To predict the ligand-binding sites on HucR, we carried out blind docking with AutoDock 4.0[35] (Scripps Research Institute) using uric acid as ligand. Among the predicted ligand-binding sites, two binding sites per monomer were selected as having the highest calculated affinity for the provided ligand. The predicted sites were mapped near the DNA-binding helix, where the inner binding site is buried in the protein and the outer binding site is mapped on the surface opposite the inner binding site. Subsequent docking of the ligand at high resolution mapped the residues directly hydrogen bonding to the ligand. All macromolecular graphics were created with PyMOL.[36] Three-dimensional protein structure alignments were carried out with TM-align[37] on Structure-Based Sequences Alignment Program§. Mutational analysis of amino acids predicted to coordinate was carried out to determine the functional significance of these residues *in vitro.*

Tryptophan fluorescence measurement

Emission spectrum was scanned from 300 nm to 360 nm with an excitation of 295 nm on a Jasco FP-6300 spectrofluorimeter at 25 °C using a 0.5 cm pathlength cuvette. Ligands were dissolved to appropriate concentrations in 0.2 M NaOH. WT and mutant proteins were resuspended in FL buffer [40 mM Tris–HCl (pH 8.0), 0.2 mM EDTA, 0.1% (wt/vol) Brij58, 100 mM NaCl, and 10 mM $MgCl_2$] to a final concentration of 0.03 mg/ml. Reactions were incubated for 2 min before fluorescence was measured. The absorbance values of FL buffer, free ligand in FL buffer, and reaction mixtures were measured from 250 nm to 360 nm to correct for the inner filter effect and for normalization of data. Correction of observed fluorescence and referred calculations were performed as described previously.[29] Briefly, inner filter effects were resolved by the following correction factor: corrected fluorescence intensity at a given wavelength $F_{corr}(\lambda) = F_c(\lambda) \times 10^{(A_{ex}/2 + A_{em}/2)}$, where $F_c(\lambda)$ is the observed fluorescence, and A_{ex} and A_{em} are the absorbance at the excitation and emission wavelengths, respectively. Percentage quenching (Q_{338}) upon ligand interaction was calculated by $Q_{338} = 1 - (F_{corr}[X]/F_{corr}[0])$, where $F_{corr}[X]$ and $F_{corr}[0]$ are corrected fluorescence intensities at 338 nm with X μM and 0 μM ligand, respectively. Fluorescence quenching data were fitted to a nonlinear binding isotherm with the Hill equation $Q_{338} = [n(1/K_d)^{n_H}(U)^{n_H}]/[1 + (1/K_d)^{n_H}(U)^{n_H}]$, where n represents the quenching plateau, U is the urate concentration, K_d is the observed dissociation constant, and n_H is the Hill coefficient.

† http://autodock.scripps.edu/
‡ http://vina.scripps.edu/index.html
§ http://www.charite.de/bioinf/strap/

Antagonistic effects of ligand binding on HucR–*HucO* interaction

The observed equilibrium dissociation constant (K_d) of WT HucR and mutants was measured by EMSA as described by Wilkinson and Grove, with slight modifications.[25] The "top" strand of *HucO* (synthetic 77mer spanning the binding region of HucR) was 5′-^{32}P end labeled with T4 polynucleotide kinase and [γ-^{32}P]ATP. The top strand was then annealed to its complement by slow cooling in TE′ with 50 mM NaCl from 90 °C to room temperature (25 °C). One femtomole of *HucO* was incubated with 0.05–20 nM HucR in a reaction mixture of 10 μl with a binding buffer containing 8% glycerol, 0.5 M Tris, 10 μM EDTA, 0.05% Brij58, and 100 μg/ml bovine serum albumin. Reactions were allowed to equilibrate for 45 min and loaded onto an 8% native gel. After electrophoresis at 8 V/cm, gels were dried and exposed to storage phosphor screens (Molecular Dynamics) and scanned with a Storm 840 phosphorimager (Amersham Pharmacia Biotech Limited). Densitometric data obtained with ImageQuant 5.1 (Molecular Dynamics) were analyzed by KaleidaGraph 4.0 (Synergy Software) using a hyperbolic curve fit of data to the equation: normalized fractional saturation of $HucO = [n(P)/K_d]/[1 + (P/K_d)]$, where n is the number of HucR binding sites and P is the free protein concentration.

The specificity of ligand binding for HucR was assayed with uric acid and several molecules from the purine degradation pathway. Selected ligands were dissolved in 0.4 M NaOH, and binding reactions were carried out in a binding buffer consisting of 0.5 M Tris (pH 8.0). WT HucR (0.6 nM) was incubated with ^{32}P-end-labeled *HucO* (0.1 nM) in the presence of increasing concentrations of selected ligands from 0.625 mM to 20 mM in a 10 μl reaction. Assessment of ligand binding antagonism by different mutants was carried out with a protein concentration equivalent to their K_d, titrated with an increasing concentration of uric acid (2.5–20 mM). Densitometric data from more than three independent experiments were statistically analyzed by fitting to a two-component exponential decay, where fractional saturation of $HucO = Ae^{-kx} + Be^{-lx}$, where k and l are equilibrium dissociation constants, x is the ligand concentration, and A and B are the minimum saturation plateaus.

Acknowledgements

We thank Dr. Marcia Newcomer for insightful discussions and the use of the spectrofluorimeter. National Science Foundation grants (MCB-0414875 and MCB-0744240 to A.G.) and an LSU Faculty Research Grant are gratefully acknowledged.

References

1. Buchmeier, N., Bossie, S., Chen, C. Y., Fang, F. C., Guiney, D. G. & Libby, S. J. (1997). SlyA, a transcriptional regulator of *Salmonella typhimurium*, is required for resistance to oxidative stress and is expressed in the intracellular environment of macrophages. *Infect. Immun.* **65**, 3725–3730.
2. Hommais, F., Oger-Desfeux, C., Van Gijsegem, F., Castang, S., Ligori, S., Expert, D. *et al.* (2008). PecS is a global regulator of the symptomatic phase in the phytopathogenic bacterium *Erwinia chrysanthemi* 3937. *J. Bacteriol.* **190**, 7508–7522.
3. Wilkinson, S. P. & Grove, A. (2006). Ligand-responsive transcriptional regulation by members of the MarR family of winged helix proteins. *Curr. Issues Mol. Biol.* **8**, 51–62.
4. Martin, R. G. & Rosner, J. L. (1995). Binding of purified multiple antibiotic-resistance repressor protein (MarR) to mar operator sequences. *Proc. Natl Acad. Sci. USA*, **92**, 5456–5460.
5. Seoane, A. S. & Levy, S. B. (1995). Characterization of MarR, the repressor of the multiple antibiotic resistance (mar) operon in *Escherichia coli*. *J. Bacteriol.* **177**, 3414–3419.
6. Sulavik, M. C., Gambino, L. F. & Miller, P. F. (1995). The MarR repressor of the multiple antibiotic resistance (mar) operon in *Escherichia coli*: prototypic member of a family of bacterial regulatory proteins involved in sensing phenolic compounds. *Mol. Med.* **1**, 436–446.
7. Alekshun, M. N. & Levy, S. B. (1999). Characterization of MarR superrepressor mutants. *J. Bacteriol.* **181**, 3303–3306.
8. Martin, R. G. & Rosner, J. L. (2004). Transcriptional and translational regulation of the marRAB multiple antibiotic resistance operon in *Escherichia coli*. *Mol. Microbiol.* **53**, 183–191.
9. Hirooka, K., Danjo, Y., Hanano, Y., Kunikane, S., Matsuoka, H., Tojo, S. & Fujita, Y. (2009). Regulation of the *Bacillus subtilis* divergent yetL and yetM genes by a transcriptional repressor, YetL, in response to flavonoids. *J. Bacteriol.* **191**, 3685–3697.
10. Kumaraswami, M., Schuman, J. T., Seo, S. M., Kaatz, G. W. & Brennan, R. G. (2009). Structural and biochemical characterization of MepR, a multidrug binding transcription regulator of the *Staphylococcus aureus* multidrug efflux pump MepA. *Nucleic Acids Res.* **37**, 1211–1224.
11. Yoshida, M., Hiromoto, T., Hosokawa, K., Yamaguchi, H. & Fujiwara, S. (2007). Ligand specificity of MobR, a transcriptional regulator for the 3-hydroxybenzoate hydroxylase gene of *Comamonas testosteroni* KH122-3s. *Biochem. Biophys. Res. Commun.* **362**, 275–280.
12. Yu, L., Fang, J. & Wei, Y. (2009). Characterization of the ligand and DNA binding properties of a putative archaeal regulator ST1710. *Biochemistry*, **48**, 2099–2108.
13. Alekshun, M. N., Levy, S. B., Mealy, T. R., Seaton, B. A. & Head, J. F. (2001). The crystal structure of MarR, a regulator of multiple antibiotic resistance, at 2.3 Å resolution. *Nat. Struct. Biol.* **8**, 710–714.
14. Bordelon, T., Wilkinson, S. P., Grove, A. & Newcomer, M. E. (2006). The crystal structure of the transcriptional regulator HucR from *Deinococcus radiodurans* reveals a repressor preconfigured for DNA binding. *J. Mol. Biol.* **360**, 168–177.
15. Chin, K. H., Tu, Z. L., Li, J. N., Chou, C. C., Wang, A. H. & Chou, S. H. (2006). The crystal structure of XC1739: a putative multiple antibiotic-resistance repressor (MarR) from *Xanthomonas campestris* at 1.8 Å resolution. *Proteins*, **65**, 239–242.
16. De Silva, R. S., Kovacikova, G., Lin, W., Taylor, R. K., Skorupski, K. & Kull, F. J. (2005). Crystal structure of the virulence gene activator AphA from *Vibrio cholerae* reveals it is a novel member of the winged helix transcription factor superfamily. *J. Biol. Chem.* **280**, 13779–13783.

17. Hong, M., Fuangthong, M., Helmann, J. D. & Brennan, R. G. (2005). Structure of an OhrR–ohrA operator complex reveals the DNA binding mechanism of the MarR family. *Mol. Cell*, **20**, 131–141.
18. Kraft, P., Oeckinghaus, A., Kummel, D., Gauss, G. H., Gilmore, J., Wiedenheft, B. *et al.* (2004). Crystal structure of F-93 from *Sulfolobus* spindle-shaped virus 1, a winged-helix DNA binding protein. *J. Virol.* **78**, 11544–11550.
19. Kumarevel, T., Tanaka, T., Nishio, M., Gopinath, S. C., Takio, K., Shinkai, A. *et al.* (2008). Crystal structure of the MarR family regulatory protein, ST1710, from *Sulfolobus tokodaii* strain 7. *J. Struct. Biol.* **161**, 9–17.
20. Lim, D., Poole, K. & Strynadka, N. C. (2002). Crystal structure of the MexR repressor of the mexRAB–oprM multidrug efflux operon of *Pseudomonas aeruginosa*. *J. Biol. Chem.* **277**, 29253–29259.
21. Miyazono, K., Tsujimura, M., Kawarabayasi, Y. & Tanokura, M. (2007). Crystal structure of an archaeal homologue of multidrug resistance repressor protein, EmrR, from hyperthermophilic archaea *Sulfolobus tokodaii* strain 7. *Proteins*, **67**, 1138–1146.
22. Saridakis, V., Shahinas, D., Xu, X. & Christendat, D. (2008). Structural insight on the mechanism of regulation of the MarR family of proteins: high-resolution crystal structure of a transcriptional repressor from *Methanobacterium thermoautotrophicum*. *J. Mol. Biol.* **377**, 655–667.
23. Newberry, K. J., Fuangthong, M., Panmanee, W., Mongkolsuk, S. & Brennan, R. G. (2007). Structural mechanism of organic hydroperoxide induction of the transcription regulator OhrR. *Mol. Cell*, **28**, 652–664.
24. Wilke, M. S., Heller, M., Creagh, A. L., Haynes, C. A., McIntosh, L. P., Poole, K. & Strynadka, N. C. (2008). The crystal structure of MexR from *Pseudomonas aeruginosa* in complex with its antirepressor ArmR. *Proc. Natl Acad. Sci. USA*, **105**, 14832–14837.
25. Wilkinson, S. P. & Grove, A. (2004). HucR, a novel uric acid-responsive member of the MarR family of transcriptional regulators from *Deinococcus radiodurans*. *J. Biol. Chem.* **279**, 51442–51450.
26. Kahn, K. & Tipton, P. A. (1998). Spectroscopic characterization of intermediates in the urate oxidase reaction. *Biochemistry*, **37**, 11651–11659.
27. Gabison, L., Chiadmi, M., Colloc'h, N., Castro, B., El Hajji, M. & Prange, T. (2006). Recapture of [*S*]-allantoin, the product of the two-step degradation of uric acid, by urate oxidase. *FEBS Lett.* **580**, 2087–2091.
28. Raychaudhuri, A. & Tipton, P. A. (2002). Cloning and expression of the gene for soybean hydroxyisourate hydrolase. Localization and implications for function and mechanism. *Plant Physiol.* **130**, 2061–2068.
29. Wilkinson, S. P. & Grove, A. (2005). Negative cooperativity of uric acid binding to the transcriptional regulator HucR from *Deinococcus radiodurans*. *J. Mol. Biol.* **350**, 617–630.
30. Cox, M. M. & Battista, J. R. (2005). *Deinococcus radiodurans*—the consummate survivor. *Nat. Rev. Microbiol.* **3**, 882–892.
31. Goodsell, D. S., Morris, G. M. & Olson, A. J. (1996). Automated docking of flexible ligands: applications of AutoDock. *J. Mol. Recognit.* **9**, 1–5.
32. Gabison, L., Prange, T., Colloc'h, N., El Hajji, M., Castro, B. & Chiadmi, M. (2008). Structural analysis of urate oxidase in complex with its natural substrate inhibited by cyanide: mechanistic implications. *BMC Struct. Biol.* **8**, 32.
33. Dawson, R. M. C., Elliott, D. C., Elliott, W. H. & Jones, K. M. (1986). Spectral data and pK_a values for purines pyrimidines nucleosides and nucleotides. In *The Data for Biochemical Research* (pp. 103–114), Clarendon Press, Oxford.
34. Morris, G. M., Huey, R. & Olson, A. J. (2008). Using AutoDock for ligand–receptor docking. *Current Protocol in Bioinformatics*, chapt. 8, pp. 14; unit 8, John Wiley & Sons, Inc., Malden, MA.
35. Huey, R., Morris, G. M., Olson, A. J. & Goodsell, D. S. (2007). A semiempirical free energy force field with charge-based desolvation. *J. Comput. Chem.* **28**, 1145–1152.
36. DeLano, W. L. (2008). *The PyMOL Molecular Graphics System*. DeLano Scientific, Palo Alto, California, USA.
37. Zhang, Y. & Skolnick, J. (2005). TM-align: a protein structure alignment algorithm based on the TM-score. *Nucleic Acids Res.* **33**, 2302–2309.